Accepted Manuscript

In Vitro Culture Increases Mechanical Stability of Human Tissue Engineered Cartilage Constructs by Prevention of Microscale Scaffold Buckling

Jill M. Middendorf, Sonya Shortkroff, Caroline Dugopolski, Stephen Kennedy, Joseph Siemiatkoski, Lena R. Bartell, Itai Cohen, Lawrence J. Bonassar

In Vitro Culture Increases Mechanical Stability of Human Tissue Engineered Cartilage Constructs by Prevention of Microscale Scaffold Buckling

Jill M. Middendorf[1], Sonya Shortkroff[2], Caroline Dugopolski[2], Stephen Kennedy[2], Joseph Siemiatkoski[2], Lena R. Bartell[3], Itai Cohen, PhD[3,4], Lawrence J. Bonassar, PhD[1,5]

[1]Sibley School of Mechanical and Aerospace Engineering, Cornell University, Ithaca, NY
[2]Histogenics Corporation, Waltham, Massachusetts
[3]Department of Applied Engineering and Physics, Cornell University, Ithaca, NY
[4]Department of Physics, Cornell University, Ithaca, NY
[5] Meinig School of Biomedical Engineering, Cornell University, Ithaca, NY

*Address Correspondence to:
Lawrence J. Bonassar, PhD.
Professor
Department of Biomedical Engineering
149 Weill Hall
Cornell University
Ithaca, NY 14853
Phone: (607) 255-9381
Fax: (607) 255-7330
lb244@cornell.edu

Key Words Cartilage Repair, Microscale Mechanics, Compression, Buckling, Tissue Engineering

Word Count: 3500

1

Abstract

Many studies have measured the global compressive properties of tissue engineered (TE) cartilage grown on porous scaffolds. Such scaffolds are known to exhibit strain softening due to local buckling under loading. As matrix is deposited onto these scaffolds, the global compressive properties increase. However the relationship between the amount and distribution of matrix in the scaffold and local buckling, is unknown. To address this knowledge gap, we studied how local strain and construct buckling in human TE constructs changes over culture times and GAG content. Confocal elastography techniques and digital image correlation (DIC) were used to measure and record buckling modes and local strains. Receiver operating characteristic (ROC) curves were used to quantify construct buckling. The results from the ROC analysis were placed into Kaplan-Meier survival function curves to establish the probability that any point in a construct buckled. These analysis techniques revealed the presence of buckling at early time points, but bending at later time points. An inverse correlation was observed between the probability of buckling and the total GAG content of each construct. This data suggests that increased GAG content prevents the onset of construct buckling and improves the microscale compressive tissue properties. This increase in GAG deposition leads to enhanced global compressive properties by prevention of microscale buckling.

Introduction

The poor intrinsic repair capabilities of native articular cartilage has driven interest in tissue engineered constructs. Several tissue engineered cartilage techniques embed cells onto a 3D porous scaffold that allows for tissue growth (Brittberg, 2010; Hunziker et al., 2015). Such techniques have been successful clinically (Brittberg, 2010; Kon et al., 2013), filling the defect, maintaining cell viability, and inducing new matrix growth (Willers et al., 2005). However, biological markers alone are not enough to understand the success of such implants. Notably, FDA guidance advises measuring the mechanical properties of these implants to better understand their function (U.S. Food and Drug Administration, 2011).

The global compressive properties of tissue engineered cartilage implants using porous cell seeded 3D scaffolds have been well documented. A variety of scaffold materials, scaffold shapes, cell types, and growth conditions affect the compressive properties of the constructs (Temenoff and Mikos, 2000). The compressive modulus vary widely from about 2% to nearly 90% of the native values (Cigan et al., 2016; Paschos et al., 2017; Peng et al., 2014; Rosenzweig et al., 2013; Tang et al., 2013). In many studies, an increase in proteoglycans (GAG) content was correlated with an improved compressive moduli (Griffin et al., 2016; Klein et al., 2007; Mauck et al., 2002; Middendorf et al., 2017). However, the mechanical interactions between newly deposited GAG and the porous scaffold are not well understood.

A number of studies have linked the compressive behavior of porous scaffold materials to their microscale structure. Under small compressive strains, porous materials such as honeycomb scaffolds, exhibit linear stress-strain behavior associated with a slight bending of the pore walls (Gibson and Ashby, 1997). At higher strains, the stress-strain curve enters a plateau region, where the walls become unstable and buckle. The onset of buckling in these porous structures

3

can be changed by increasing wall thickness or depositing material within the pores(Gibson and Ashby, 1997; Slivka et al., 2001). Both of these phenomena strengthen the porous structure and may thus explain changes in the compressive mechanics of tissue engineered cartilage due to matrix deposition into pores or on scaffold surfaces. This matrix synthesis is expected to locally reinforce the scaffold and thus increase the strain needed to induce buckling. However, the amount of matrix synthesis required to reinforce the scaffold to delay buckling is unknown.

In addition to the total amount of matrix deposition, the location of matrix in the scaffold may also influence the local buckling. Matrix deposition on porous scaffolds is highly heterogeneous(Klein et al., 2007; Krase et al., 2014; Middendorf et al., 2017). Previously, extensive matrix deposition on the outside edges of the scaffold with less deposition on the inside pore surfaces has been shown. Scaffold pores with more matrix deposition reinforce the scaffold, while scaffold pores with little or no matrix deposition may create local weaknesses. Local structural variations caused by matrix deposition will affect the global compressive properties. However, the relationship between microscale compressive mechanics, the GAG content and the onset of buckling in tissue engineered constructs has not been studied. Techniques to measure the local strain in native and tissue engineered cartilage have been recently developed(Buckley et al., 2010, 2008), but these techniques have not been applied to identifying the local compressive mechanics and buckling.

The goal of this study was to understand how GAG deposition influences the microscale compressive properties of tissue engineered cartilage with respect to scaffold buckling. In this study, we examined an implant similar to NeoCart®, made of a 3D collagen type I honeycomb scaffold seeded with human chondrocytes. NeoCart is currently in advanced human clinical trials and has shown good integration and defect filling (Crawford et al., 2012, 2009). In previous

studies, the global compressive modulus of cultured implants improved with increased culture and improved with increased GAG content (Middendorf et al., 2017). However, the microscale mechanism behind this improvement is unknown. To better understand this mechanism, the current study identified the local strain and local scaffold buckling in tissue engineered constructs as a function of culture times and identified the relationship between local buckling and GAG content.

Methods

Tissue Construct Preparation

Human tissue engineered cartilage constructs were prepared as described previously (Crawford et al., 2012, 2009). Briefly, cadaveric normal human cartilage tissue from the femoral condyles of a 28 year old male was obtained under protocol from National Disease Research Interchange (NDRI, Philadelphia, Pa), then processed by enzymatic digestion with collagenase (Worthington Biochemical, Lakewood, NJ) to yield chondrocytes. Chondrocytes were isolated, expanded in DMEM/F12 culture medium containing 10% fetal bovine serum (Gibco, Thermo Fisher Scientific, Waltham, MA) through passage 1 at 37°C under 5% CO_2, suspended in a 3 mg/mL type I collagen solution (PureCol, Advanced Biomatrix, San Diego, CA) at a concentration of $5x10^6$ cells/mL, and seeded into approximately 6 mm diameter by 1.5 mm thick type 1 collagen honeycomb scaffolds (Itoh et al., 2001)(Koken, Tokyo, Japan). Both the scaffold and the collagen solution were produced from bovine. Constructs were incubated at 37°C, 5% CO_2, and 2% O_2 in static culture with media changes at regular intervals. Constructs were removed from culture at multiple stages of development (1, 3, 5, and 7 weeks post seeding) and stored at -20ºC. A total of 22 constructs were produced by this process and allocated for compression testing described below, with 4-7 constructs tested at each time point (1, 3, 5, and 7 weeks).

5

Compressive Strain Mapping

The compressive modulus of constructs was obtained using a modified version of a previously established protocol (Buckley et al., 2010, 2008). Briefly, constructs were bisected longitudinally into hemi-cylinders then stained with 14 μg/ml 5-dichlorotriazinyl-aminofluorescein (5-DTAF, Molecular Probes1, Grand Island, NY) for 30 minutes followed by a 20 minute rinse in PBS with protease inhibitors (Figure 1 A1). Constructs were mounted between two plates on a tissue deformation imaging stage (TDIS, Figure A2) and placed on an inverted Zeiss LSM 510 5 live confocal microscope and imaged using a 488 nm laser. Constructs were compressed to 10% axial strain (Figure 1 A2).

The microscale Lagrange strain measured under compressive loading was determined using digital image correlation (DIC) implemented in MATLAB (Figure 1 A3) (Eberl, 2010; Jones and Jones, 2015). The software was set to track local deformation fields on a 78.7 μm grid with a correlation area of 160 x 160 μm. The microscale axial, transverse, and shear strains at each point were calculated by interpolating the microscale displacements using a finite element shape function. Depth-dependent strain data was calculated by averaging all strain values at a given depth.

Buckling Identification

Since we expect to see local buckling in these constructs, we visually distinguished between bending and buckling (Figure 1 A4). All observed deformation was elastic. However, bending is characterized by a single long-wavelength arc spanning the length of the image. Buckling is visually classified as a complete sine wave with a small wavelength, less than 400 μm (initial pore size ranged from 200 to 400μm). The visual characterization of these constructs was then used to establish quantitative differences between buckling and bending. To understand

6

general trends and detailed responses, construct buckling and mechanical behavior was compared on the global and local scale respectively.

Global Buckling Identification

Global buckling analysis was used to establish a connection between the distribution of construct strains and buckling. A construct was considered buckled based on a threshold identified by examining the strain and strain rate histograms. To accomplish this a training data set consisting of 8 constructs (4 with buckling and 4 without buckling) was used in a statistical model to identify a threshold to apply to remaining constructs. This model used receiver operating characteristic (ROC) curves to identify a threshold that can distinguished between buckling and bending in constructs. First, histograms of the 3 strains (axial, transverse, and shear) and 3 strain rates (axial, transverse, and shear) were created from the training data set (Figure 1 B1). Because buckling is more likely to occur at higher strains, the strain and strain rate values at 3 percentiles (50th, 75th, and 85th) were recorded. These values were then placed into a receiver operating characteristic (ROC) curve (Streiner and Cairney, 2007) such that a total of 18 curves were created (3 strain and 3 strain rate at each of the 3 percentiles, Figure 1 B2). In a ROC curve the sensitivity (y axis) indicates the ability of the threshold value to correctly predict buckling and the specificity (x axis) indicates the ability of the threshold value to correctly predict bending. The area under the curve (AUC) for each ROC curve was used to determine the percentile and strain or strain rate values that created the best ROC curve. An AUC equal to one indicates the data fits the ROC curve perfectly and an AUC equal to 0.5 indicates a random data fit. Once the best ROC curve fit was determined, the best threshold value was established using the 'closest to the top left' method (Streiner and Cairney, 2007). The resulting threshold was applied to all remaining constructs to determine if a construct underwent

7

buckling or bending. The validity of this technique was checked by visually inspecting for buckling or bending. The difference between using the buckling threshold and visually inspecting the constructs was recorded (Figure 1 B3).

Local Buckling Identification

To complement the global buckling analysis, the local relationship between strain and buckling was analyzed to provide a more detailed understanding of the relationship between strain and buckling. The local buckling analysis identified a local buckling threshold using ROC curves, then applied this threshold to remaining constructs. First, 6 constructs (3 constructs that visually exhibited buckling and 3 constructs that visually exhibited bending) were chosen for analysis. Three strain (axial, transverse, and shear) and 3 strain rates (axial, transverse, and shear) were recorded at each DIC grid point on each of the 6 constructs (Figure 1 C1). The strain and strain rate values were recorded at 4 global compressive strains (2.5%, 5%, 7.5%, and 10%). Each grid point on the 6 constructs was visually labeled as buckling (Y) or bending (N) using visual analysis. The bending or buckling mode and the strain/strain rate at each grid point was used to create six ROC curves (Figure 1 C2). Once the best ROC curve was determined, the best threshold value was identified using the 'closest to the top left' method (Figure1 C2). The threshold value then was applied to all constructs at 4 global compressive strains. This technique's validity was tested by comparing the results of a visual inspection on an additional 2 constructs to the results from the local threshold (Figure 1 C3).

Biochemical Analysis

After confocal imaging, constructs were analyzed for GAG content as a measure of cartilage matrix synthesis. Constructs were weighed, lyophilized, and weighed again to obtain construct weight. Then, constructs were papain digested at 60°C for 14 hours. Sulfated GAG

8

content was measured using a dimethylmethylene blue (DMMB) assay (Enobakhare et al., 1996).

Statistical Analysis

A Kaplan-Meier survival analysis was used to determine the probability that any grid point in a construct underwent buckling based on application of the local buckling threshold. All correlations were determined using a linear regression. Regressions were considered significant with $p < 0.05$.

Results

Compression of Constructs

First we investigated how construct microscale compressive properties progressed with increased culture. Videos were recorded of constructs during compression to 10% axial strain. Video analysis revealed buckling in 1 week constructs at both 5% and 10% global axial compression (Figure 2A, Supplement Material). The buckled areas occurred at random depths from the construct surface. High axial strain occurred at these random depths ($E_{xx} \approx 20\text{-}25\%$) as seen in the 1 week construct strain maps.

As the constructs matured buckling decreased and the global axial strain at which this buckling mode occurred increased. In 3 week constructs, buckling occurred at 10% global axial strain (Figure 2B, Supplement Material). The buckled areas still occurred at random depths with areas of high axial strain ($E_{xx} \approx 20\text{-}25\%$). Constructs grown for 5 weeks buckled less, indicating a transition to bending (Figure 2C, Supplement Material). After 7 weeks, constructs did not buckle, even at 10% axial strain (Figure 2D, Supplemental Material). The surface of these constructs exhibited higher axial strain than the deeper in the tissue (7 week construct strain maps).

9

Global Analysis of Buckling

We established a buckling threshold to quantitatively identify buckled constructs. An ROC curve using histogram strain and strain rate percentiles was used to identify this global buckling threshold (Figure 3A). The transverse strain (E_{yy}) at the 75th percentile provided the highest AUC (AUC = 1, Figure 3B) and therefore best distinguishes between a construct with bending and a construct with buckling. A threshold value of $E_{yy} = 3.2\%$ was chosen using the 'closest to the top left' method (Figure 3C). Therefore, if the transverse strain at the 75th percentile was greater than 3.2% the construct was considered buckled. This buckling threshold provided exact correlation in the training data set. This threshold was applied to all remaining constructs and verified by visual inspection. All 1 and 7 week constructs were correctly identified. Overall 77% of the 22 constructs were correctly identified as buckled (Supplemental Material).

Based on the compressive videos, buckling was believed to correlate with areas of high axial strain. Therefore, we plotted the depth dependent axial strain of each construct and identified each construct as undergoing either buckling or bending on this plot using the global buckling threshold. In 1 week constructs, high axial strain occurred at random tissue depths (Figure 4A). These areas of high axial strain were associated with buckled locations. All 1 week constructs exhibited buckling. After 3 weeks, the location of high axial strain began to shift toward the surface of the construct (Figure 4B). Three of the five 3 week constructs exhibited buckling. Similarly, at 5 weeks, areas of high axial strain continued to shift toward the construct surface (Figure 4C). Two of the five 5-week constructs exhibited buckling. In 7 week constructs, areas of high axial strain were concentrated on the surface (Figure 4D). Zero 7 week constructs exhibited buckling. Using this analysis we observed a shift in the areas of high axial strain. In

10

buckled constructs, high strain occurred at random depths while constructs with only bending

exhibited high strain at the construct surface.

Local Analysis of Buckling

Another quantitative buckling measure was established to investigate the mechanics at

buckled locations using ROC curves containing local strain and strain rates. Two strains, axial

strain (E_{xx}) and transverse strain (E_{yy}), fit the ROC well with similar high AUC (AUC_{Eyy} = 0.76,

AUC_{Exx} = 0.78, Figure 5B). The remaining 4 parameters (E_{xy}, $\dot{E}_{xx}$, $\dot{E}_{xy}$, and $\dot{E}_{yy}$) fit the ROC

curves poorly (AUC ≈ 0.5 to 0.7). Therefore, the two best fit ROC curves (E_{xx} and E_{yy}) were

analyzed to identify the best threshold value. The best threshold value for local buckling was the

transverse strain, E_{yy} = 2.0%, because the shortest distance to the top left on the transverse strain

ROC curve (0.12) was less than the shortest distance to the top left (0.13) on the axial strain

ROC curve (Figure 5C). The buckling threshold, E_{yy} = 2.0% was applied to all grid points on

remaining constructs, such that any grid point with a transverse strain greater than 2.0% was

considered buckled. This local buckling threshold was verified on two constructs (one with

buckling and one with bending). The threshold correctly identified 85% of all grid points on the

two additional constructs (Supplemental Material).

The results from the local buckling analysis can predict the likelihood of buckling at any

grid point in a construct. A Kaplan-Meier survival function found the probability that any point

in a construct buckled. As expected, this probability was highest after 1 week in culture and

lowest after 7 weeks in culture at every global axial strain value (Figure 6A). One week

constructs were two times more likely to exhibit bulking than 7 week constructs.

After axial testing, the probability of buckling was related to a biological construct

maturation parameter: GAG content. The GAG content, measured using DMMB, was plotted

11

against the probability that any grid point on the construct buckled (Figure 6B). At all four global strains the probability of buckling was negatively correlated with construct GAG content. Constructs with low GAG content (< 10 µg/mg) had a high probability of buckling especially at 10% axial strain (probabilities ranging from 25% to 95%). Constructs with high GAG content (> 40 µg/mg) had a low probability of buckling, as low as 2.1% with most below 50%. Increased global strain increased the probability of buckling, while increased maturation decreased the probability of buckling.

Discussion

This study identified interactions between local scaffold buckling, local strain, and GAG content in tissue engineered constructs over a range of culture times. During culture, construct behavior under compression changed from buckling at early time points to bending at later time points. Buckling was associated with areas of high strain observed at random depths throughout the constructs. The relationship between the microscale compressive strain, buckling, and the GAG content was also identified in this study. At early time points, constructs with less GAG content were more likely to buckle. In contrast, as the construct matured, the probability of buckling decreased with increased GAG deposition. Collectively, this data suggests that GAG deposition prevents construct buckling and improves the microscale compressive tissue properties.

GAG deposition also changed the depth at which maximal axial strain occurred in constructs. Initially, the scaffolds consisted of pores ranging from 200-400 µm (Figure 7A). This variability in the scaffold structure likely resulted in variations in wall thickness, which in turn create areas of local weakness. During culture, heterogeneous GAG deposition lines the inner scaffold surfaces (Figure 7C) (Krase et al., 2014; Middendorf et al., 2017), which reinforces the

12

walls enough to overcome local weaknesses. GAG content also concentrates on the outside edges of the construct (Figure 7B). The highly concentrated, GAG-rich regions on the construct surface are very compliant under compression. The shift in the depth at which high axial strain occurred indicates how variability in the scaffold and localization of GAG deposition could change the construct's mechanical behavior.

To fully understand why the probability of buckling decreased with increased GAG content, we considered classic mechanics buckling theories. Two different theories adequately explain this system. The first theory requires the GAG content and GAG deposition to increase the ratio of pore wall thickness to wall width by lining the inner scaffold surfaces (Figure 7C), where wall width refers to the distance between the nodes connecting multiple walls. Increasing this ratio increases the strain required for the onset of buckling (Gibson et al., 2010). Since the onset of buckling is proportional to the square of the ratio of wall thickness to wall width, eventually the construct will never leave the elastic region. This theory requires the GAG and ECM deposition on the inner scaffold walls to have approximately the same modulus as the initial scaffold. The second theory requires the construct to behave similar to a set of tubes (honeycomb scaffold) filled with a compliant core (GAG rich substance, Figure 7D). The compliant core supports the outer tube under compression, increasing the resistance to buckling (Gibson et al., 2010). This theory requires a sufficiently stiff inner core to act as an elastic foundation. Both theories provide evidence that might explain why an increase in the total GAG content correlated with a decreased probability of buckling. However a quantitative study on the local GAG and collagen content is necessary to fully understand buckling.

A major challenge to tissue engineered cartilage is understanding the level of construct maturity required for implantation. In both lab experiments and clinical trials maturity is

typically assessed using GAG content or global compressive properties. These parameters do not define any distinct changes in microstructural features. The identification of buckling, a distinct on-off phenomenon, can define distinct changes in microstructure and characterize implant maturity. In this study, constructs required an adequate pore fill to prevent buckling at 10% axial strain. Similarly, the location of GAG (Figure 7) with relation to the scaffold is believed to have changed the local mechanics and buckling. Since the total GAG content and Safranin-O staining does not fully explain the microscale mechanics and onset of buckling, more complex criteria such as quantifying local ECM content may be necessary to predict the implant maturity and function.

In this study GAG content and location played an important role in determining the microscale compressive properties of tissue engineered constructs. However, some studies have identified collagen content as an important aspect of tissue engineered cartilage. A large change in collagen content is necessary to improve the compressive properties of tissue engineered cartilage by a small amount (Griffin et al., 2016). A large change in collagen content is unlikely to occur during the short 7 weeks of culture. Therefore, collagen was not measured. Additionally, various growth parameters such as seeding density, scaffold structure, and growth media could change the amount and type of ECM deposited, and the onset of buckling. Seeding density and the growth parameters in this study were chosen to match NeoCart, a tissue engineered construct in advanced clinical trials. Finally, the relationship between local ECM components and microscale mechanics of constructs is not well understood. Future studies using the techniques described in this study and either FTIR or Raman spectroscopy can determine the relationship between local ECM (Kunstar et al., 2013; Rieppo et al., 2012)and local mechanics (Silverberg et al., 2014).

We measured changes in the microscale compressive properties of human chondrocyte-seeded collagen constructs during maturation. Results indicate the amount and location of GAG content influence buckling. Since the constructs tested in this study are similar to a tissue engineered construct (NeoCart) that is currently in advanced human trials (Crawford et al., 2012, 2009), the study provided insight regarding the microscale mechanical properties that change the global function of a successful implant. Allowing adequate ECM deposition prior to implantation prevents buckling. Prevention of buckling improves the compressive properties and global function of human constructs.

Acknowledgments

Conflicts of Interest

S.K, S.S, and C.D. are full time employees and stock holders of Histogenics Corp. J.S. is a consultant for Histogenics Corp. J.M. and L.J.B., were partially funded by an award from Histogenics to Cornell University.

Brittberg, M., 2010. Cell carriers as the next generation of cell therapy for cartilage repair: a review of the matrix-induced autologous chondrocyte implantation procedure. Am. J. Sports Med. 38, 1259–1271. doi:10.1177/0363546509346395

Buckley, M.R., Bergou, A.J., Fouchard, J., Bonassar, L.J., Cohen, I., 2010. High-resolution spatial mapping of shear properties in cartilage. J. Biomech. 43, 796–800. doi:10.1016/j.jbiomech.2009.10.012

Buckley, M.R., Gleghorn, J.P., Bonassar, L.J., Cohen, I., 2008. Mapping the depth dependence of shear properties in articular cartilage. J. Biomech. 41, 2430–7. doi:10.1016/j.jbiomech.2008.05.021

Cigan, A.D., Roach, B.L., Nims, R.J., Tan, A.R., Albro, M.B., Stoker, A.M., Cook, J.L., Vunjak-Novakovic, G., Hung, C.T., Ateshian, G.A., 2016. High seeding density of human chondrocytes in agarose produces tissue-engineered cartilage approaching native mechanical and biochemical properties. J. Biomech. 49, 1909–1917. doi:10.1016/j.jbiomech.2016.04.039

Crawford, D.C., DeBerardino, T.M., Williams, R.J., 2012. NeoCart, an autologous cartilage tissue implant, compared with microfracture for treatment of distal femoral cartilage lesions: an FDA phase-II prospective, randomized clinical trial after two years. J. Bone Joint Surg. Am. 94, 979–89. doi:10.2106/JBJS.K.00533

Crawford, D.C., Heveran, C.M., Cannon, W.D., Foo, L.F., Potter, H.G., 2009. An autologous cartilage tissue implant NeoCart for treatment of grade III chondral injury to the distal femur: prospective clinical safety trial at 2 years. Am. J. Sports Med. 37, 1334–1343. doi:10.1177/0363546509333011

Eberl, C., 2010. Digital image correlation and tracking [WWW Document].

Enobakhare, B.O., Bader, D.L., Lee, D. a, 1996. Quantification of sulfated glycosaminoglycans in chondrocyte/alginate cultures, by use of 1,9-dimethylmethylene blue. Anal. Biochem. 243, 189–191. doi:10.1006/abio.1996.0502

Gibson, L.J., Ashby, M.F., 1997. Cellular Solids: Structure and Properties, 2nd ed. Cambridge University Press, Cambridge, UK.

Gibson, L.J., Ashby, M.F., Harley, B.A., 2010. Cellular Materials in Nature and Medicine. Cambridge University Press, Cambridge, UK.

Griffin, D.J., Ortved, K.F., Nixon, A.J., Bonassar, L.J., 2016. Mechanical properties and structure-function relationships in articular cartilage repaired using IGF-I gene-enhanced chondrocytes. J. Orthop. Res. 34, 149–153. doi:10.1002/jor.23038

Hunziker, E.B., Lippuner, K., Keel, M.J.B., Shintani, N., 2015. An educational review of cartilage repair: precepts & practice – myths & misconceptions – progress & prospects. Osteoarthr. Cartil. 23, 334–350. doi:10.1016/j.joca.2014.12.011

Itoh, H., Aso, Y., Furuse, M., Noishiki, Y., Miyata, T., 2001. A Honeycomb Collagen Carrier for Cell Culture as a Tissue Engineering Scaffold 25, 213–217.

Jones, E.M.C., Jones, E., 2015. Documentation for Matlab-based DIC code 1–42.

Klein, T.J., Chaudhry, M., Bae, W.C., Sah, R.L., 2007. Depth-dependent biomechanical and biochemical properties of fetal, newborn, and tissue-engineered articular cartilage. J. Biomech. 40, 182–190. doi:10.1016/j.jbiomech.2005.11.002

Kon, E., Filardo, G., Di Matteo, B., Perdisa, F., Marcacci, M., 2013. Matrix assisted autologous chondrocyte transplantation for cartilage treatment: A systematic review. Bone Joint Res. 2, 18–25. doi:10.1302/2046-3758.22.2000092

Krase, A., Abedian, R., Steck, E., Hurschler, C., Richter, W., 2014. BMP activation and Wnt-

signalling affect biochemistry and functional biomechanical properties of cartilage tissue engineering constructs. Osteoarthr. Cartil. 22, 284–292. doi:10.1016/j.joca.2013.11.011

Kunstar, A., Leferink, A.M., Okagbare, P.I., Morris, M.D., Roessler, B.J., Otto, C., Karperien, M., van Blitterswijk, C.A., Moroni, L., van Apeldoorn, A.A., 2013. Label-free Raman monitoring of extracellular matrix formation in three-dimensional polymeric scaffolds. J. R. Soc. Interface 10, 20130464. doi:10.1098/rsif.2013.0464

Mauck, R.L., Seyhan, S.L., Ateshian, G.A., Hung, C.T., 2002. Influence of seeding density and dynamic deformational loading on the developing structure/function relationships of chondrocyte-seeded agarose hydrogels. Ann. Biomed. Eng. 30, 1046–1056. doi:10.1114/1.1512676

Middendorf, J.M., Griffin, D.J., Shortkroff, S., Dugopolski, C., Kennedy, S., Siemiatkoski, J., Cohen, I., Bonassar, L.J., 2017. Mechanical properties and structure-function relationships of human chondrocyte-seeded cartilage constructs after in vitro culture. J. Orthop. Res. 1–9. doi:10.1002/jor.23535

Paschos, N., Lim, N., Hu, J.C., Athanasiou, K.A., 2017. Functional properties of native and tissue-engineered cartilage toward understanding the pathogenesis of chondral lesions at the knee . A bovine. J. Orthop. Res. doi:10.1002/jor.23558

Peng, G., McNary, S.M., Athanasiou, K.A., Reddi, A.H., 2014. Surface Zone Articular Chondrocytes Modulate the Bulk and Surface Mechanical Properties of the Tissue Engineered Cartilage. Tissue Eng. Part A 20, 3332–41. doi:10.1089/ten.tea.2014.0099

Rieppo, L., Rieppo, J., Jurvelin, J.S., Saarakkala, S., 2012. Fourier transform infrared spectroscopic imaging and multivariate regression for prediction of proteoglycan content of articular cartilage. PLoS One 7. doi:10.1371/journal.pone.0032344

Rosenzweig, D.H., Chicatun, F., Nazhat, S.N., Quinn, T.M., 2013. Cartilaginous constructs using primary chondrocytes from continuous expansion culture seeded in dense collagen gels. Acta Biomater. 9, 9360–9369. doi:10.1016/j.actbio.2013.07.024

Silverberg, J.L., Barrett, A.R., Das, M., Petersen, P.B., Bonassar, L.J., Cohen, I., 2014. Structure-function relations and rigidity percolation in the shear properties of articular cartilage. Biophys. J. 107, 1721–1730.

Slivka, M. a, Leatherbury, N.C., Kieswetter, K., Niederauer, G.G., 2001. Porous, resorbable, fiber-reinforced scaffolds tailored for articular cartilage repair. Tissue Eng. 7, 767–780. doi:10.1089/107632701753337717

Streiner, D.L., Cairney, J., 2007. What's Under the ROC? An Introduction to Reciever Operating Characteristics Curves. Can. J. Psychiatry 52, 121–128. doi:10.1177/070674370705200210

Tang, C., Xu, Y., Jin, C., Min, B.H., Li, Z., Pei, X., Wang, L., 2013. Feasibility of autologous bone marrow mesenchymal stem cell-derived extracellular matrix scaffold for cartilage tissue engineering. Artif Organs 37, E179-90. doi:10.1111/aor.12130

Temenoff, J.S., Mikos, a G., 2000. Injectable biodegradable materials for orthopedic tissue engineering. Biomaterials 21, 2405–2412. doi:10.1016/S0142-9612(00)00108-3

U.S. Food and Drug Administration, 2011. Guidance for Industry: Preparation of IDEs and INDs for Products Intented to Repair or Replace Knee Cartilage, www.FDA.gov.

Willers, C., Chen, J., Wood, D., Xu, J., Zheng, M.H., 2005. Autologous Chondrocyte Implantation with Collagen Bioscaffold for the Treatment of Osteochondral Defects in Rabbits. Tissue Eng. 11, 1065–1076.

Figure 1

Overview of the sample preparation and buckling analysis. A1) constructs were cut in half then stained with DTAF. A2) Videos were recorded of construct compression to 10% axial strain. A3) Videos were analyzed using a DIC software. A4) Buckling modes were visually identified and labeled both globally and locally. B1) The global buckling analysis identified the 50th, 75th, and 85th percentile of strain/strain rate histograms (one strain/strain rate histogram per construct). B2) Recorded values and visual buckling information were placed into ROC curves to identify the best threshold. B3) The global buckling threshold was verified with the remaining 17 constructs. C1) The local buckling analysis was completed on 6 constructs by examining the buckling mode and strain/strain rate at each location in the grid. C2) Data was then placed into an ROC curve to determine the best threshold. C3) The threshold was verified by examining 2 additional constructs.

Figure 2

The axial strain of individual constructs at multiple time points while under axial compression A) After 1 week in culture axial compression videos show areas of high axial strain and compressive failure (inserts indicate areas of buckling, black arrows indicate areas of high strain with buckling). B) At 3 weeks in culture construct buckling is less pronounced than in 1 week construct. Buckling began at higher axial strains than 1 week constructs C) After 5 weeks constructs begin to form a thin surface layer of proteoglycans with no construct buckling. C) 7 week constructs show resistance to compressive failure and a compliant surface associated with a thicker layer of proteoglycans.
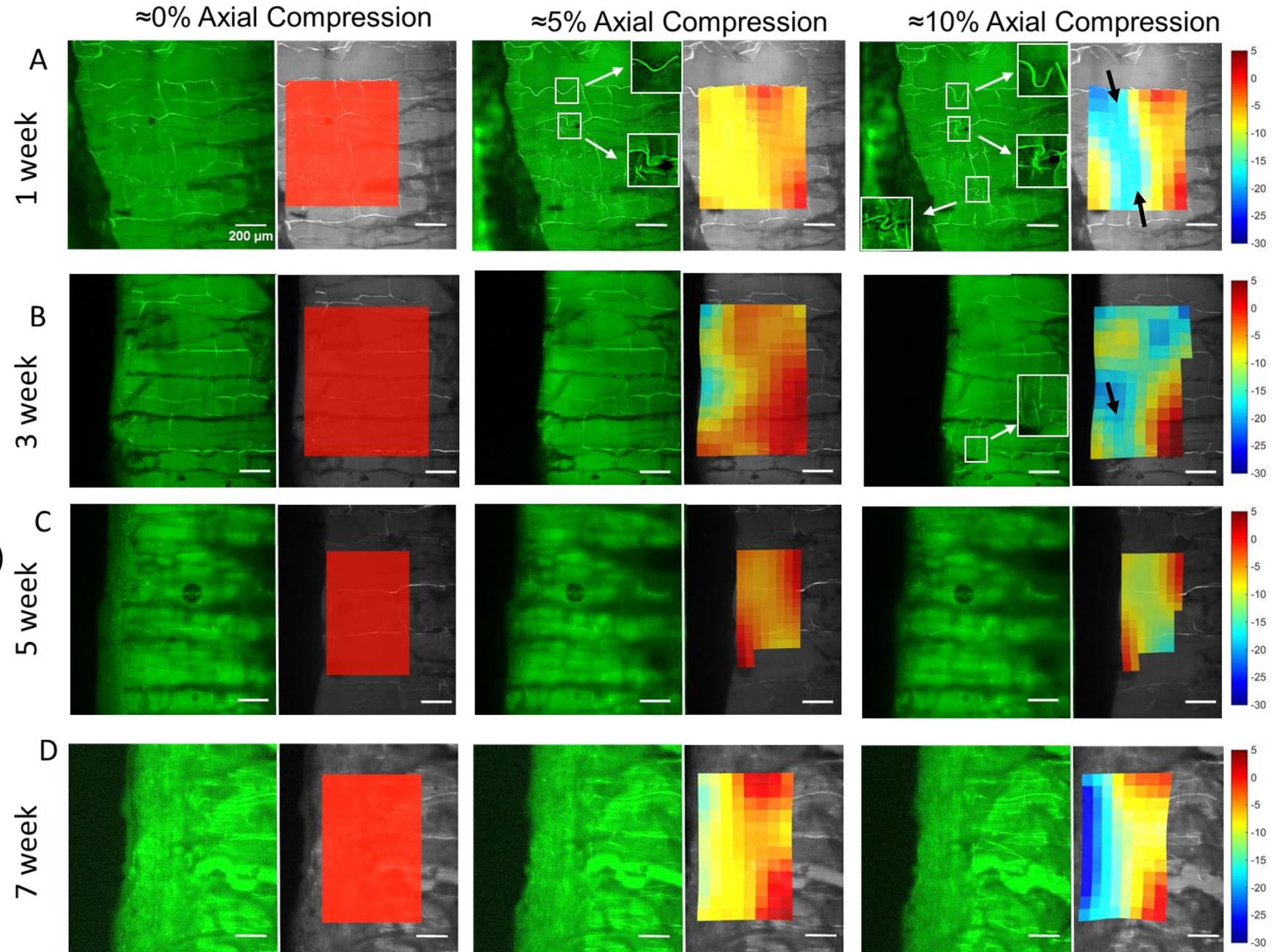
Figure 3
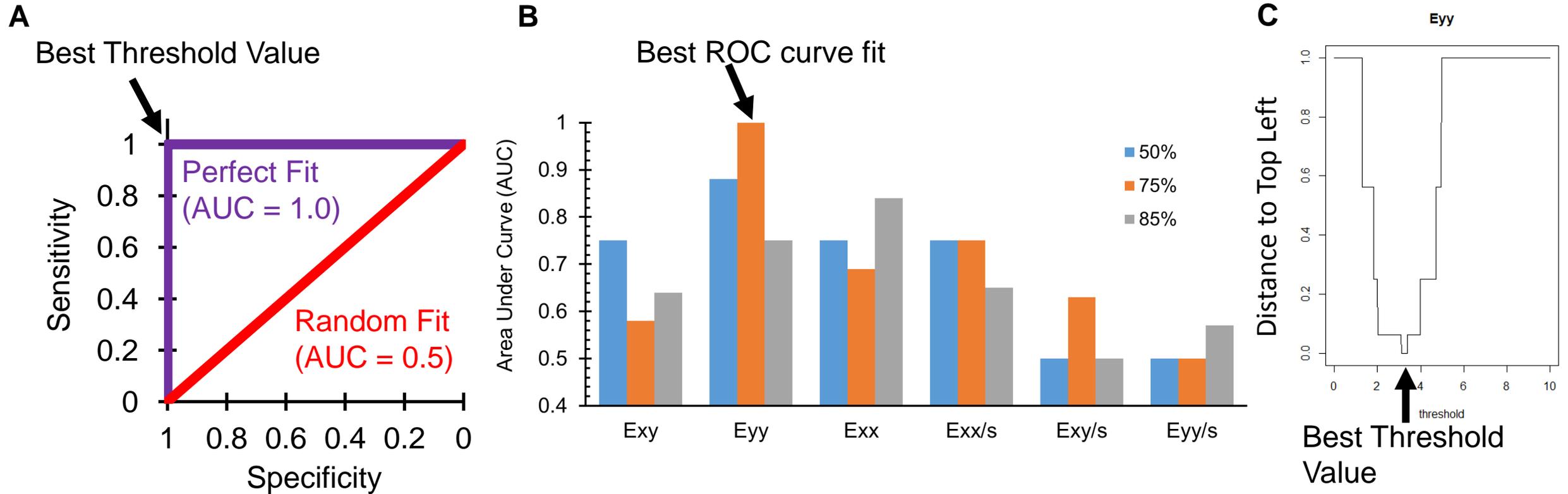
A) Representative image showing a perfect ROC and a ROC with random data. The best threshold value can be found using the "closest to the top left" method, which finds the value that minimizes the distance to the top left of the ROC using least squares analysis. B) After plotting the ROC curves the AUC can be calculated and compared for each strain and strain rate examined at each percentile. The highest AUC identifies the parameter that fits the ROC the best. In this study the transverse strain (E_{yy}) at the 75th percentile provides the best fit to the ROC curve. C) When the distance to the top left of the ROC curve is plotted versus all possible threshold values, we can easily identify the best threshold value of E_{yy} = 3.2%. Collectively this data indicate that when the top 25% of transverse strains exceed 3.2%, the construct will experience local buckling.

Figure 4

The axial strain versus depth of individual constructs at multiple time points while under axial compression After 1 week in culture axial compression videos show random areas of high axial strain that correspond to the areas of buckling. All constructs exhibited buckling after 1 week in culture. After 7 weeks constructs show resistance to buckling. A compliant surface zone associated with a thicker layer of proteoglycans was revealed. All constructs exhibited buckling. At 3 and 5 week in culture constructs exhibited characteristics of both 1 and 7 week construct.
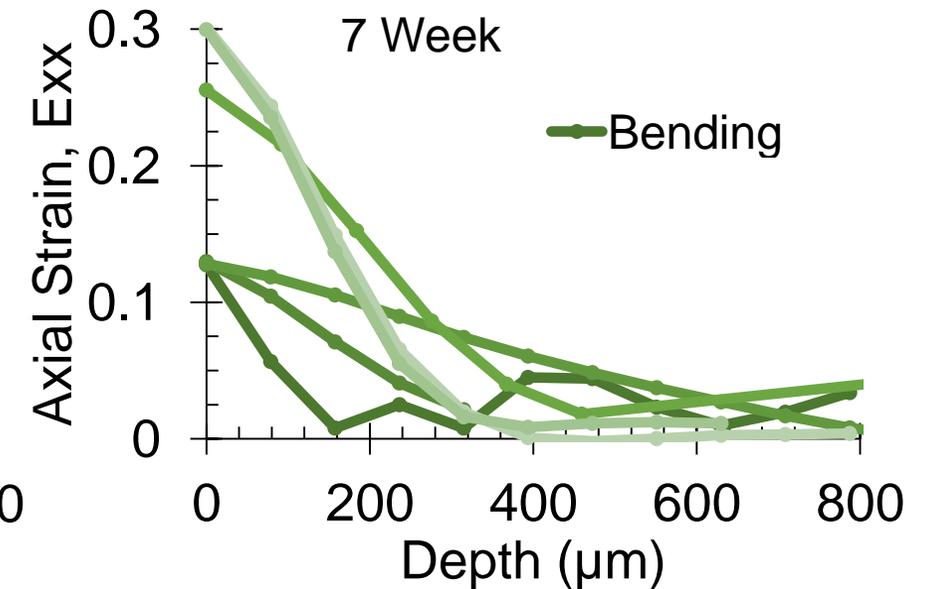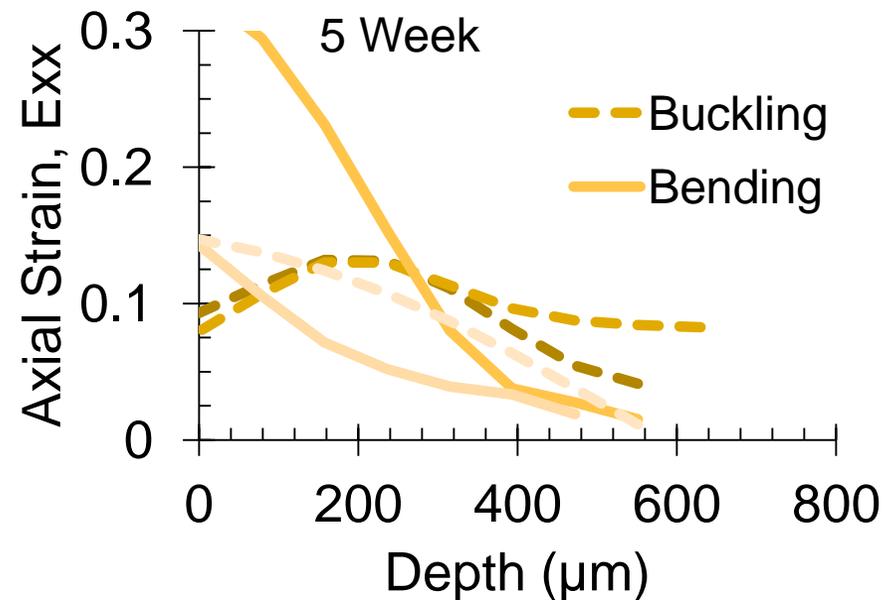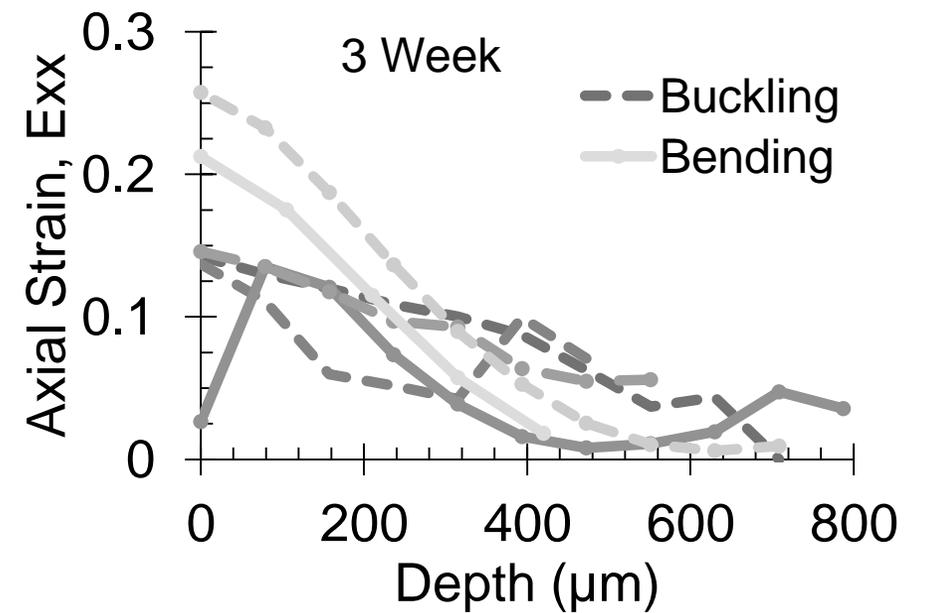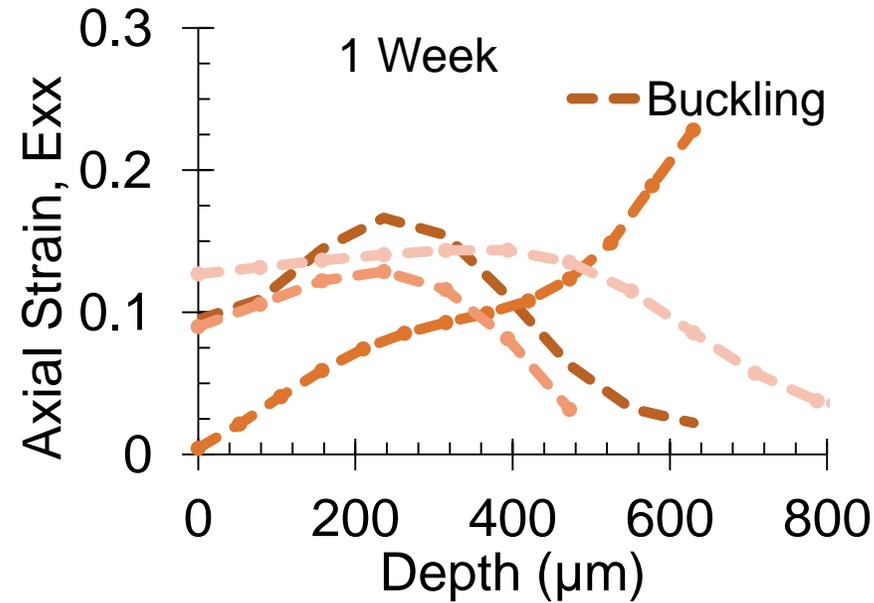
Figure 5

A) Representative image showing a portion of the displacement grid on a buckled construct. Each grid point was visually inspected and labeled Y (yes buckling) or N (no bending). B) After creating ROC curves for each variable tested the AUC can be compared. Both the axial strain (E_{xx}) and transverse strain (E_{yy}) fit the ROC curve well. C) Analysis of the two data sets that fit the ROC the best are plotted using the "least squares method." This method found the transverse strain provided a better threshold value (E_{yy}) than the axial strain (E_{xx}).

A

N	Y	Y	Y	N	N	N	N	N
N	N	Y	Y	Y	N	N	N	N
N	N	Y	Y	Y	N	N	N	N
N	Y	Y	Y	Y	Y	N	N	N
N	Y	Y	Y	Y	N	N	N	N
N	Y	Y	Y	Y	Y	N	N	N

B

Two strains fit the ROC well

C

Axial Strain, E_{xx}

Threshold (E_{xx}) = 8.7%
Y Value = 0.13

Transverse Strain, E_{yy}

Threshold (E_{yy}) = 2.0%
Y Value = 0.12
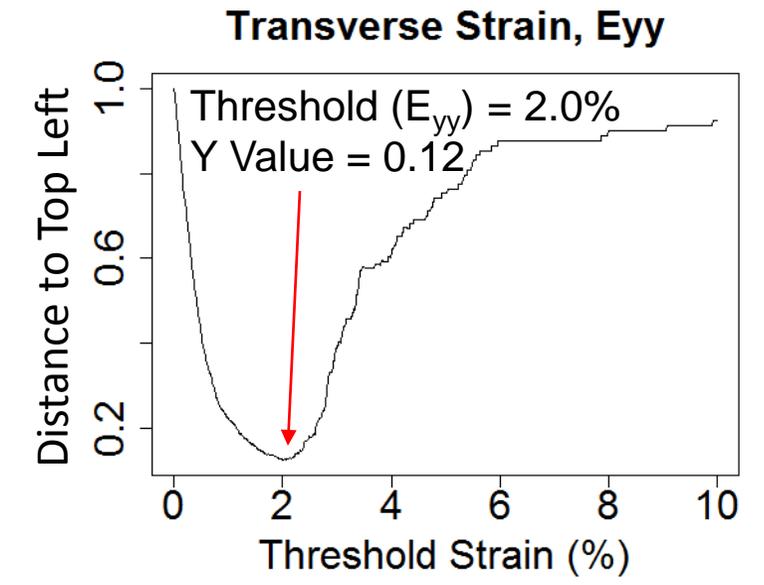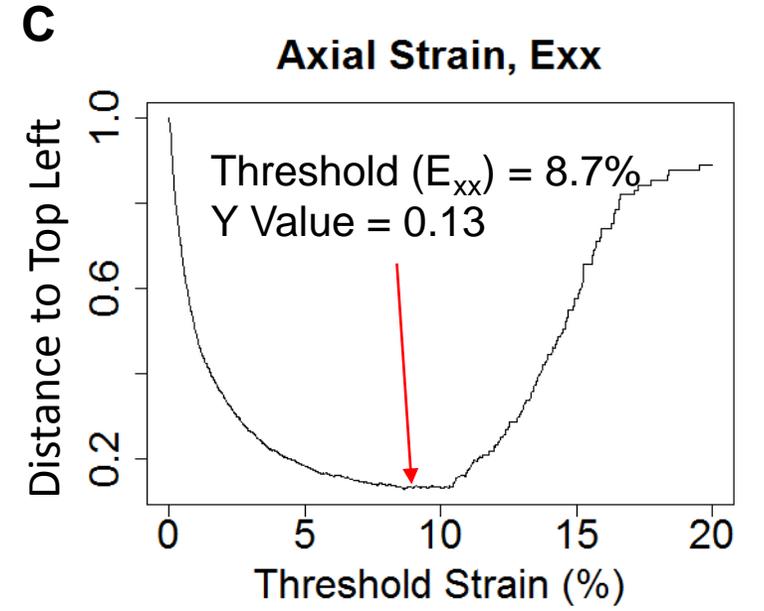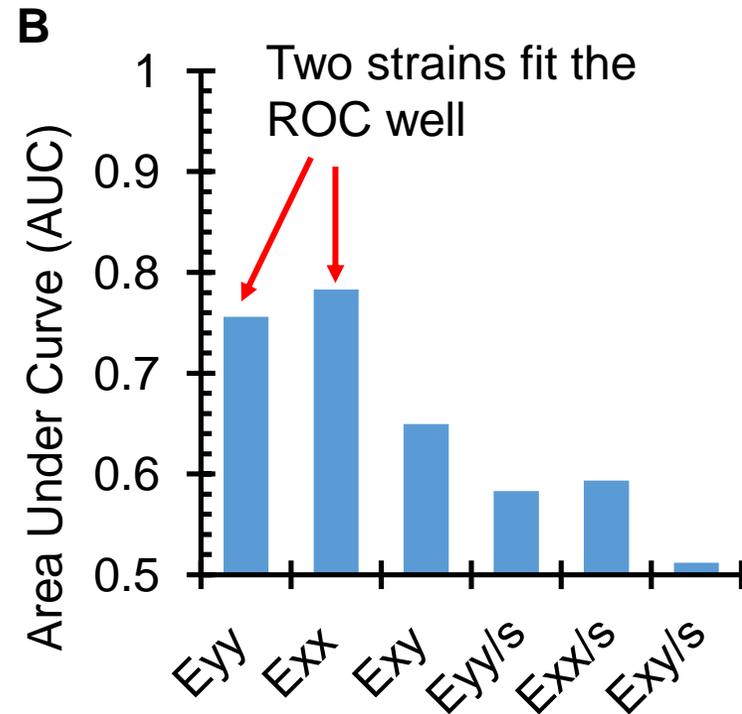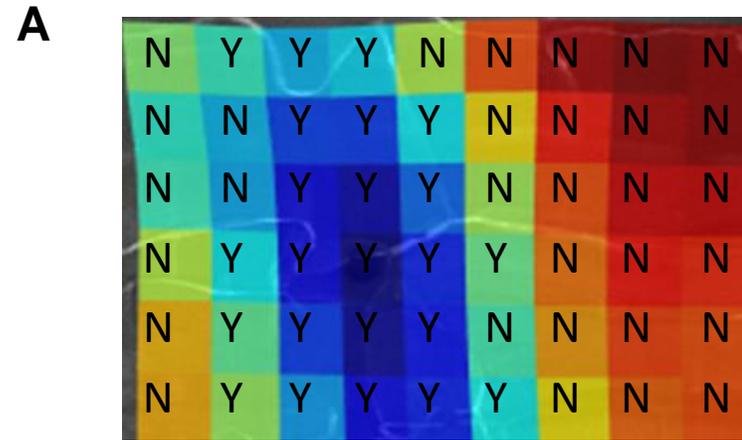
Figure 6
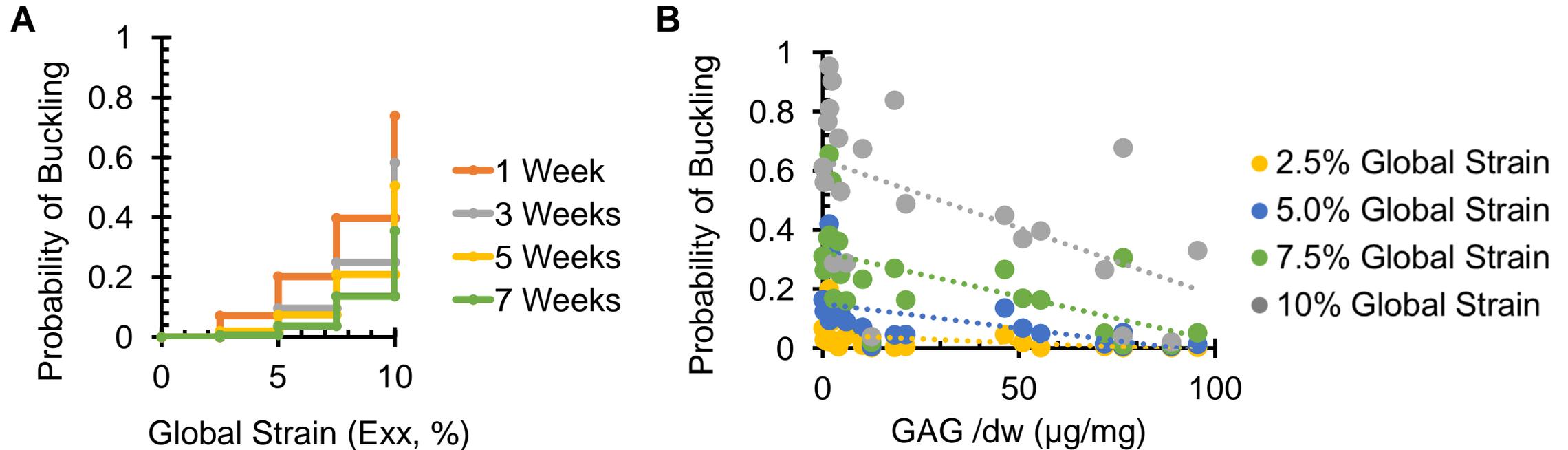
A) Using a Kaplan Meier survival function the probability that any grid point on a construct at a specific time point can be calculated and plotted versus the bulk axial strain. The curves for each time point are statistically different from each other with 1 week constructs being the most likely to undergo buckling and 7 week constructs being the least likely to undergo buckling. B) When the probability of buckling on a given construct is plotted vs the bulk GAG content of that construct, linear correlations are observed. The strongest linear correlation occurred at 10% bulk strain (p = 0.008) and the weakest correlation occurred at 2.5% bulk axial strain (p = 0.06)
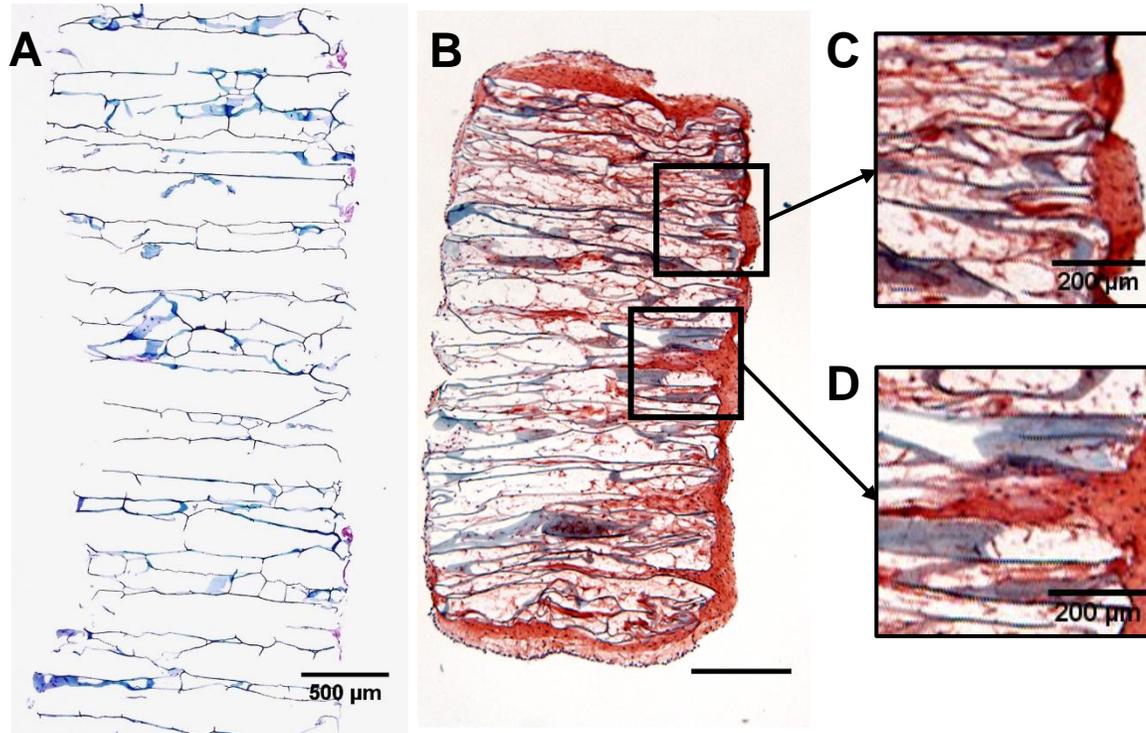
Representative safranin-O staining of the cross section of tissue engineered constructs. A) At early time points constructs are collagen honeycomb structures with little GAG. B) As constructs mature, GAG content is highly concentrated on the outside edges of the scaffold. C) GAG content may line the inner pores or D) fill the inner pores of the scaffold.